PHYSICS AND CHEMISTRY OF SOLID STATE
V. 26, No.4 (2025) pp. 738-751
Section: Chemistry

DOI: 10.15330/pcss.26.4.738-751

Vasyl Stefanyk Carpathian National University

ФІЗИКА І ХІМІЯ ТВЕРДОГО ТІЛА
Т. 26, № 4 (2025) С. 738-751
Хімічні науки

PACS: 81.16.Hc; 81.16.Pr

ISSN 1729-4428 (Print)
ISSN 2309-8589 (Online)

V.V. Husak, V.V. Shvadchak, L.M. Soltys

Catalyst-Assisted H_2O_2 Systems for Bacterial Disinfection of Wastewater: From UV/Visible Synergy to Electro-/Photo-Fenton Pathways

Vasyl Stefanyk Carpathian National University, Ivano-Frankivsk, Ukraine, viktor.husak@cnu.edu.ua

Hydrogen peroxide assisted advanced oxidation processes are pivotal for next-generation water treatment, yet progress is slowed by fragmented evidence, non-uniform metrics, and scale-up blind spots. This review consolidates mechanisms and performance across homogeneous and heterogeneous Fenton and photo-Fenton catalysts, including Prussian blue analogues, MOF-derived oxides and carbons, and spinels, as well as peroxidase-like nanozymes, carbon co-catalysts, and photolytic UV/H_2O_2 and visible or solar routes. We harmonize conditions through a benchmarking scheme that combines energy per order, oxidant utilization efficiency, photon-normalized kinetics, mineralization selectivity, and durability with leaching tests. Kinetic mapping pinpoints limitations involving H_2O_2 activation versus self-scavenging, metal redox cycling, mass transfer, and pH or matrix effects from bicarbonate, halides, and natural organic matter. We address by-product control and safety through staged oxidant delivery, matrix-aware pretreatment, and in situ H_2O_2 generation in electro-Fenton systems. Screening techno-economic and life-cycle indicators delineates regimes where UV/H_2O_2 is favored, where solar photo-Fenton narrows the energy gap, and where photoelectrochemical architectures extend durability. From these insights we propose design rules for materials, reactors, and operation, and we outline reporting standards that couple photon accounting, stability protocols, and transparent cost and impact metrics to enable fair comparisons and faster translation.

Keywords: Hydrogen peroxide, Advanced oxidation processes, Photo-Fenton catalysis, UV/H_2O_2, Wastewater treatment.

Received 04 April 2025; Accepted 29 October 2025.

Content

Abbreviations

AOP, AOPs: Advanced oxidation process or processes.
ARB: Antibiotic-resistant bacteria.

ARG, ARGs: Antibiotic resistance gene or genes.
BOD: Biochemical oxygen demand.
CB: Conduction band.
CFU: Colony-forming units.
COD: Chemical oxygen demand.
DFT: Density functional theory.
DOC: Dissolved organic carbon.
EPR: Electron paramagnetic resonance.
g-C_3N_4: Graphitic carbon nitride.
ICP-MS: Inductively coupled plasma mass spectrometry.
LAS: alkylbenzene sulfonate.
LCA: Life Cycle Assessment.
MOF, MOFs: Metal–organic framework or frameworks.
NOM: Natural organic matter.
PB: Prussian blue.
PBA, PBAs: Prussian blue analogue or analogues.
PEF: Photoelectro-Fenton.
PMS: Peroxymonosulfate.
qPCR, PCR: Quantitative polymerase chain reaction and polymerase chain reaction.
RCS: Reactive chlorine species.
ROS: Reactive oxygen species.
TOC: Total organic carbon.
VB: Valence band.
XPS: X-ray photoelectron spectroscopy.
XRD: X-ray diffraction.

Introduction

Conventional biological and physicochemical treatments frequently fail to fully remove bacterial contaminants from water. Chlorination remains widely used despite the formation of disinfection by-products and other drawbacks [1]. Advanced oxidation processes (AOPs) offer an environmentally friendly alternative by generating highly reactive oxygen species (ROS), predominantly hydroxyl radicals (HO•), that disinfect and mineralize organics [1]. Representative AOPs include ozonation, UV/H_2O_2, Fenton and photo-Fenton reactions, photocatalysis, sonolysis, electrochemical oxidation, and their hybrids [1].

Among AOPs, the photo-Fenton process (light/Fe/H_2O_2) is particularly attractive because it is simple, low-cost, and effective against viruses, protozoa, spore-forming bacteria, fungi, and yeasts. The corresponding reaction network is initiated by H_2O_2 photolysis and is followed by radical propagation and termination to benign products (H_2O, O_2) as summarized in Fig. 1. Under irradiation, Fe^{3+}/Fe^{2+} cycling accelerates HO• production, while ROS attack proteins, lipids, and nucleic acids, causing oxidative lesions, strand breaks, and structural damage to DNA. The ability to use sunlight, the low reagent demand for H_2O_2, and the abundance of natural Fe^{3+} make photo-Fenton a promising option for virus inactivation in water [1].

Natural waters can exhibit photo-Fenton-like behavior without added H_2O_2. Study [2] demonstrated that Fe ions (especially Fe^{2+}) in the presence of natural organic matter (NOM) can induce solar water disinfection (SODIS) at pH 5–8. Formation of Fe^{3+}–NOM complexes keeps Fe^{3+} dissolved and photoactive, shifts NOM absorption to longer wavelengths, and promotes ligand-to-metal charge-transfer, facilitating photoreduction to Fe^{2+}. This accelerates Fe^{2+}/Fe^{3+} cycling and boosts production of photochemically produced reactive intermediates, notably $^1O_2$, thereby improving light-driven bacterial inactivation [2].

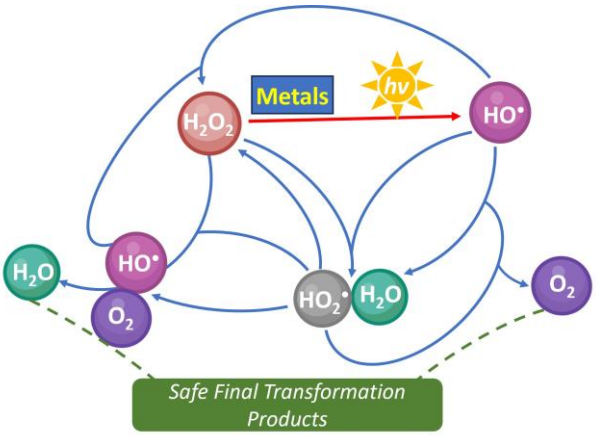

Fig. 1. Photolysis- and Metal-Catalyzed Radical Pathways of H_2O_2 in the Photo-Fenton Process. The red arrow denotes the primary step (H_2O_2 + hν → HO•), while blue arrows trace propagation and interconversion among H_2O_2, HO•, and HO_2•. Green dashed arrows mark termination routes yielding benign end-products – H_2O and O_2. The scheme highlights that under irradiation, the H_2O_2 radical network self-quenches to safe final transformation products, a key feature of advanced oxidation processes.

Together, the evidence indicates that (i) HO• is the primary oxidant in Fenton-type systems, (ii) light greatly accelerates ROS generation and disinfection kinetics, with additional gains from iron chelation (e.g., EDDS), (iii) in

natural waters, a photo-Fenton-like route to germicidal ROS can occur even without external H_2O_2 due to the presence of Fe complexes with organic compounds. These insights motivate AOP designs that leverage sunlight, appropriate iron speciation, and H_2O_2 dosing to drive the radical network in Fig. 1 toward rapid pathogen inactivation while terminating to safe products.

This work aims to build an integrated mechanism-grounded review of recent results in H_2O_2-assisted advanced oxidation processes in water and wastewater treatment. We overviewed homogeneous and heterogeneous Fenton/photo-Fenton systems, including Prussian blue and spinels; peroxidase-like nanozymes and carbon co-catalysts, considering photolytic UV/H_2O_2 and visible/solar-driven routes. By coupling kinetic analysis with comparative performance indicators (mineralization selectivity, catalyst durability) and sustainability lenses (by-product control), we establish clear benchmarks in order to harmonize disparate operating conditions and metrics. The goal is to distill actionable design rules and reporting standards that guide materials selection, reactor engineering (photoelectrochemical and electro-Fenton), and safe, renewable-powered, and modular deployment from bench to full scale.

I. Homogeneous catalysts

Homogeneous Fenton-like catalysts are widely investigated for the degradation of organic pollutants because they efficiently generate hydroxyl radicals (HO•) from hydrogen peroxide. Transition-metal ions such as Fe^{2+}/Fe^{3+}, Cu^{2+}, and Co^{2+} afford high catalytic activity under mild conditions; however, a narrow operational pH window, metal leaching, and difficult post-treatment recovery constrain practical deployment. These limitations motivate chelation strategies and hybrid process designs that stabilize iron, expand pH tolerance, and couple oxidation with separation.

Solar photo-Fenton has shown promising performance at the community scale. A metagenomic study [3] showed that solar illumination using 30 mg L^{-1} Fe^{2+} and 50 mg L^{-1} H_2O_2 for 240 min with intermittent iron addition strongly decreased microbial richness and diversity in municipal wastewater treatment plant effluent, removing up to 86% of major phyla. It was more effective than solar illumination in the presence of H_2O_2 only or H_2O_2 alone and completely eliminated clinically relevant pathogens (*e.g.*, *Staphylococcus*, *Enterococcus*, *Pseudomonas*, *Stenotrophomonas, Klebsiella*). However, enrichment of *Proteobacteria*, which are frequent carriers of antibiotic resistance genes (ARGs), was observed and warrants further investigation. Nearly 60% of ARGs related to sulfonamides, macrolides, and tetracyclines were removed, while β-lactam- and fluoroquinolone-associated ARGs were fully eliminated, highlighting solar photo-Fenton as a candidate measure against antimicrobial resistance in tropical regions [3]. These outcomes are consistent with the light-driven radical network in Fig. 1 and are schematized in Fig. 2.

Whether conventional Fenton and photo-Fenton generate distinct ROS pools has been debated. A recent study [4] compared Fenton, photo-Fenton, and photo-Fenton in the presence of EDDS (ethylenediamine-N,N′-disuccinic acid, a biodegradable iron chelator) reactions for inactivation of antibiotic-resistant bacteria (ARB) and degradation of carbamazepine (CBZ). In the dark and in the absence of a catalyst, ARB removal was negligible. Conventional Fenton achieved 4.37-log ARB inactivation (i.e. 4.37 order of magnitude change). Illumination dramatically enhanced performance: >6.45-log ARB inactivation was reached within 15 min for photo-Fenton and within 10 min for EDDS-modified photo-Fenton [4]. In the absence of scavengers, ARB inactivation reached 4.37-log in 30 min with Fenton, 6.48-log in 15 min with photo-Fenton, and 10 min with EDDS-modified photo-Fenton; CBZ removal followed the same trend (~80% at 30 min for Fenton vs. ~99% for photo-Fenton at 20 min and EDDS-modified photo-Fenton at 10 min) [4]. Isopropanol quenching of HO• reduced both ARB and CBZ removal (to ~2.62–5.26-log and 55–81% after 30 min), confirming HO• as the dominant oxidant across all three systems, with $^1O_2$ and $O_2^{\bullet-}$ contributing only marginally; H_2O_2 itself aided bacterial inactivation under light [4]. Kinetic analysis further underscored the advantage of light-driven systems (k_{max} = 0.11 min^{-1} for Fenton vs. 0.82 min^{-1} for photo-Fenton and 0.88 min^{-1} for EDDS-modified photo-Fenton) and showed shorter lag times when irradiation was employed [4]. These findings align with the photochemical initiation and radical propagation pathways highlighted in Fig. 1.

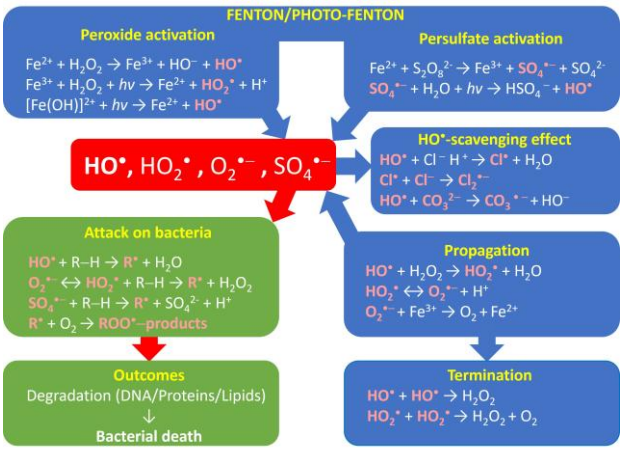

Fig. 2. Reaction network of Fe-assisted advanced oxidation processes leading to bacterial inactivation. The scheme summarizes Fenton/photo-Fenton and persulfate routes that build a common pool of primary reactive oxygen species – HO•, $HO_2^{\bullet}$, $O_2^{\bullet-}$, $SO_4^{\bullet-}$. In peroxide activation, Fe^{2+}/Fe^{3+} cycles with H_2O_2, accelerated by light, generate HO•; in persulfate activation, Fe^{2+} produces $SO_4^{\bullet-}$, which in water can further yield HO•. A HO•-scavenging effect by chloride and carbonate diverts reactivity into less aggressive halogen/carbonate radicals and moderates the overall oxidation strength. Propagation steps interconvert ROS and regenerate Fe^{2+}, while termination reactions consume radicals to H_2O_2 and O_2. In an attack on bacteria, these ROS abstract hydrogen or withdraw electrons from lipids, proteins, and DNA, initiating peroxidation and oxidative damage. The process culminates in the outcome of cellular degradation and bacterial death.

Chelation with biodegradable ligands broadens the operating space of the photo-Fenton approach. Fe–EDDS activates persulfate to produce sulfate radicals ($SO_4^{\bullet-}$) and degrades 4-tert-butylphenol across pH 4–8. EDDS complexation stabilizes Fe^{3+}, overcoming the acid requirement typical of Fe-based persulfate activation [5]. This approach allows to use of longer irradiation wavelengths ($\lambda < 580$ nm) and lowers costs. Matrix anions modulate efficacy: chloride can promote $HO^{\bullet}$ pathways and enhance degradation, whereas carbonate suppresses rates via formation of low-reactivity $CO_3^{\bullet-}$ ($k \approx 10^7\ M^{-1}\ s^{-1}$) [5]. These findings highlight the dual role of ubiquitous anions in modulating AOP efficiency: chloride can enhance, while carbonates inhibit, contaminant removal (Fig. 2). In sum, Fe-EDDS-driven persulfate activation shows strong potential for water treatment under environmentally relevant conditions. However, the effects of coexisting ions must be carefully considered when designing AOP-based wastewater treatment strategies. Collectively, these examples illustrate how homogeneous catalysis enhanced with iron ion stabilization can drive the radical pathways of organic material destruction. However, the difficulty of the separation of the catalyst remains the main limitation for the wide practical application of homogeneous catalysis in water treatment, which can be solved by the application of heterogeneous techniques.

II. Heterogeneous Fenton-like catalysts

Heterogeneous Fenton-like catalysts are attractive for degrading recalcitrant organic pollutants because they can be separated and reused, reducing secondary contamination relative to homogeneous systems [6]. Their performance depends on accessible active sites, crystallinity and defect chemistry, surface acid–base properties, electron-transfer pathways, and resistance to metal leaching. Current design routes emphasize iron (hydr)oxides engineered for rapid Fe^{3+}/Fe^{2+} cycling, spinel ferrites that combine redox activity with magnetic separability, Prussian blue (PB) and related cyanide-bridged frameworks with built-in redox networks, and metal–organic framework (MOF) platforms or derivatives offering high surface area and tunable active sites [6]. Mechanistic pathways and ROS speciation align with the network in Fig. 2, in which $HO^{\bullet}$, $HO_2^{\bullet}/O_2^{\bullet-}$, and $SO_4^{\bullet-}$ are generated, propagated, and quenched.

Ceria-modified ferrihydrite ($yCeO_2$/Fh) synthesized via a bio-template route markedly outperformed pristine ferrihydrite for tetracycline (TC) removal, achieving 98.7% degradation and 70.1% mineralization across a broad pH range, with $^{\bullet}OH$ as the dominant species [7]. The Ce^{3+}/Ce^{4+} couple accelerated Fe^{2+}/Fe^{3+} regeneration and promoted photo-electron production; the catalyst was effective in municipal/river waters and against other organics. Conductive carbon coupling further boosts activity; such composites delivered up to 7.1-fold higher bisphenol A degradation rates than Fh, retained stability over four cycles, and facilitated faster H_2O_2 activation via enhanced Fe redox cycling as confirmed by XPS [8].

Spinel ferrites (M = Cu, Co, Ni, Zn, Mn, etc.) provide abundant surface sites, low cost, and convenient magnetic recovery, but often suffer from fast electron–hole recombination; microstructure control, doping, and heterojunctions mitigate this limitation [9]. Yolk–shell $ZnFe_2O_4$ microspheres synthesized by a self-templated solvothermal method exhibited superior visible-light photo-Fenton activity toward TC versus solid $ZnFe_2O_4$ and α-Fe_2O_3. The difference can be attributed to a larger surface area, stronger light absorption, and efficient charge separation. The key species dominating the mechanism are $HO^{\bullet}$ and h^+ (hole). The degradation process is promoted by SO_4^{2-} and suppressed by $NO_3^-/HCO_3^-/Ca^{2+}/Mg^{2+}$ [10]. S-doped $ZnFe_2O_4$ nanoparticles prepared by facile calcination achieved >95% TC removal under visible light at pH 6–7. The catalyst can be separated magnetically and maintained > 95% activity after four cycles. Its performance depended on H_2O_2 concentration, catalyst dose, pH, and irradiance [11].

Cobalt ferrites made by a modified solvothermal method reached ~80% methylene blue removal in 140 min under visible light, consistent with an optical band gap of ~2.65 eV [12]. A $CoFe_2O_4$/g-C_3N_4 p–n heterojunction (3% $CoFe_2O_4$) achieved 98% methyl orange removal in 4 h via H_2O_2 activation and enhanced interfacial charge transfer. $HO^{\bullet}$ was identified as the primary reactive species, with a minor role for $O_2^{\bullet-}$ [13]. Cu-doped $MnFe_2O_4$ delivered 94.3% TC-HCl degradation in 30 min at pH 11 using 0.1 g L^{-1} catalyst and 50 mM H_2O_2. Its activity benefits from Fe/Mn/Cu synergy and oxygen vacancies. The key ROS that participated in the degradation were $O_2^{\bullet-}$ with the participation of $HO^{\bullet}$. Such material showed high stability and easy recyclability beyond the pH limitations of classical Fenton [14]. Mg-doped $NiFe_2O_4$ nanostructures obtained by microwave combustion exhibited >99% Rhodamine B removal under visible light with H_2O_2, with room-temperature ferromagnetism and phase evolution (α-Fe_2O_3 at higher Mg^{2+}) confirmed by XRD; particles were 20–35 nm with spherical morphology and contained Ni, Mg, Fe, and O, enabling magnetic handling [15].

Integration of AOP with separating membranes strongly enhances the applicability because it combines contaminant removal, *in-situ* oxidation, and self-cleaning [16]. In one design, a porous polyvinylidene fluoride (PVDF) support bearing a dual photo-Fenton layer grown in situ from polypyrrole (PPy) and zero-valent iron delivered multiple functions: enhanced hydrophilicity for antifouling, photothermal heating that enabled a solar evaporation rate of 1.17 kg m^{-2} h^{-1}, and complete dye degradation within 60 min of solar irradiation. The PPy layer stabilized the zero-valent iron, sustaining activity over repeated cycles and retaining 66% of the initial flux after four emulsion filtration cycles [17]. A spray-printed ceramic photo-Fenton membrane with nano-hematite (α-Fe_2O_3) operated under visible LEDs combined a high pure-water flux (55.8 kg m^{-2} h^{-1} kPa^{-1}) with up to 82% tetracycline removal at 20 mg L^{-1} and stable self-cleaning over five cycles; quenching and EPR implicated h^+, $O_2^{\bullet-}$, and $HO^{\bullet}$ as the dominant species [18]. A $NiFe_2O_4$/Tannic acid/PVDF composite imparted nanoscale roughness and superwettability (air superamphiphilicity and underwater superoleophobicity), enabling recyclable photo-Fenton

catalysis for dye degradation with H_2O_2 while achieving > 99% separation of emulsified oils at high flux and reusability [19].

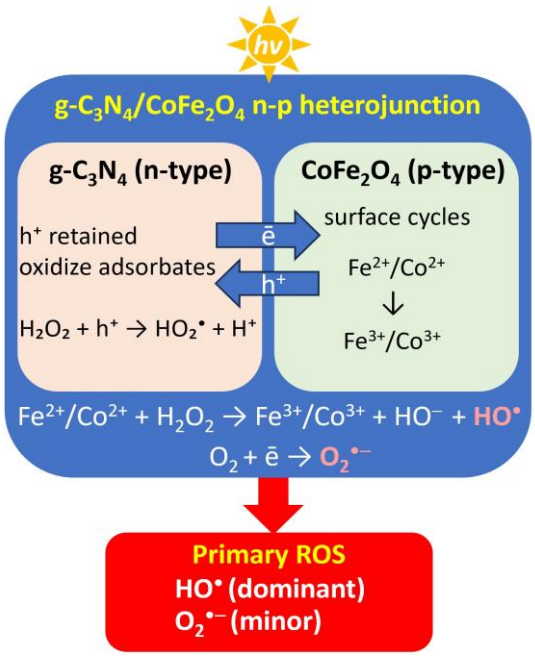

Fig. 3. g-C_3N_4/$CoFe_2O_4$ n–p heterojunction photo-Fenton catalyst.

Under illumination (hν), the n–p junction promotes directional charge separation: holes remain on g-C_3N_4 while electrons migrate to $CoFe_2O_4$. Surface $Fe^{2+}/Co^{2+} \leftrightarrow Fe^{3+}/Co^{3+}$ cycles on $CoFe_2O_4$ activate H_2O_2 to generate $HO^{\bullet}$ (dominant), and a minor pathway reduces O_2 to $O_2^{\bullet-}$. The resulting primary ROS oxidize organics/bacterial targets; the heterojunction suppresses e^-/h^+ recombination and enables efficient visible-light operation.

Prussian blue (PB), situated within the metal-organic frameworks (MOF)/coordination-polymer family, provides cyanide-bridged metal sites that facilitate multi-electron transfer and robust radical generation while allowing compositional tuning [20]. PB microcrystals with defined morphology (cubes, flowers, balls) displayed morphology-dependent activity. Hierarchical "PB-ball" showed more exposed faces, mesoporosity, higher Fe^{2+} content, and broader sunlight absorption, enabling stronger photo-Fenton/photothermal synergy [21]. Fe_3O_4@PB core–shell composites synthesized via a reactive-template method yielded a 1.5-fold higher apparent rate constant and 1.2-fold lower activation energy than Fe_3O_4 for Rhodamine B degradation. Hydroxyl radical, $HO^{\bullet}$, was shown to be the dominant oxidant. Strong magnetization (33.4 emu g^{-1}) of the catalyst enabled easy recovery and ~97.6% efficiency after five cycles [22]. Chemically reduced Prussian blue nanoparticles (13–53 nm; nanocubes and nanospheres) exhibited size-dependent solar photo-Fenton activity. The smallest particles achieved complete rhodamine B removal at pH 3 with k = 0.935 min^{-1} and 65% chemical oxygen demand mineralization, while remaining stable and non-toxic, indicating promise for scale-up [23].

MOFs offer high surface area, tunable porosity, and architected metal nodes/linkers that enable adsorption and activation of reagents in AOPs [24]. α-Fe_2O_3-x with sphere, octahedron, spindle, and rod morphologies, derived from a benzimidazole-modified Fe-MOF template, showed the highest methylene blue degradation rate for the rod-like form (k = 0.08 min^{-1}), attributed to greater surface area, enriched Fe^{2+}, and abundant oxygen vacancies that facilitate H_2O_2 dissociation and $HO^{\bullet}$ generation, as supported by density functional theory (DFT) calculations [25]. Binder-free Mn/Co MOF-derived graphite-felt cathodes (Mn_xCo_{3-x}@C-GF) achieved 99.8% removal of drug ciprofloxacin within 60 min. Mixed $Mn^{2+/3+/4+}$ and $Co^{2+/3+}$ states promoted $^{\bullet}OH$ formation via Fenton-like pathways, and the electrodes remained stable over four reuse cycles [26]. A MIL-53(Fe) photo-Fenton catalyst containing a terephthalic acid moiety, synthesized with abundant Lewis acid sites (54.26 μmol g^{-1}) delivered near-instant micropollutant removal. It allowed approximately 99% sulfamethazine elimination within 1 min at low H_2O_2 by reducing the band-gap energy and enhancing charge separation. Immobilization into a PVDF support enabled efficient removal of structurally diverse pharmaceuticals at environmentally relevant concentrations [27].

Heterogeneous Fenton-like catalysts are characterized by (i) accelerated Fe redox cycling through dopants/defects, conductive backbones, or heterojunctions; (ii) light-assisted pathways that extend activity to visible light, (iii) a wide working pH range; (iv) practical processability and recovery via magnetism, core–shell architectures, or supported films. Future work should balance high fluxes of $^{\bullet}OH/^{\bullet}O_2^-/SO_4^{\bullet-}$ with minimal leaching, sustain performance in complex matrices containing carbonate, nitrate, and hardness ions, and verify long-cycle stability and life-cycle impacts under realistic water chemistries.

III. Nanozymes and carbon-based co-catalysts (peroxidase-like)

Peroxidase-like nanozymes are attractive alternatives to natural enzymes because they are stable, inexpensive, and tunable. Pairing them with carbon supports or co-catalysts such as graphene, carbon nanotubes, or carbon dots increases electron transport and exposes more active sites, which improves H_2O_2 decomposition and raises reactive oxygen species yields for environmental and biomedical uses [28].

Carbon dots (CDs) act as enzyme mimics that are easy to synthesize, store, and recycle. Their activity can be enhanced and tuned by heteroatom doping [29]. For example, Fe-doped green-emitting CDs catalyze H_2O_2-driven oxidation of 3,3′,5,5′-tetramethylbenzidine (TMB), and inhibition by bacterial catalase enables rapid colorimetric detection of *Staphylococcus aureus* with a limit of detection of 2×10^3 CFU mL^{-1}; the same platform supports simple visual antibiotic susceptibility testing [30].

Mn-doped CDs show oxidase-like activity. They can use dissolved O_2 to convert TMB to its oxidized form. Further reduction of this form by ascorbic acid can be used for sensitive ascorbic acid quantification with a detection

limit down to 9 nM in real samples [31]. Systematic variation of Mn precursors demonstrates that Mn and N co-doping raises activity through effective metal incorporation and higher fractions of graphitic and pyridinic nitrogen, enabling sensitive TMB oxidation in the presence of H_2O_2 [32].

Single-atom Fe–N–C (Fe–N_x in a nitrogen-doped carbon matrix) prepared with a soft template provides large mesopores, high surface area, and atomically dispersed Fe. A combination of such properties delivers strong peroxidase-like conversion of H_2O_2 to $^{\bullet}OH$ and allows near-infrared photothermal boosting for antibacterial action [33]. A related one-pot route yields multifunctional Fe–NC single-atom nanozymes with oxidase, peroxidase, and catalase mimetic functions, while the conjugated N-doped carbon offers superoxide dismutase-like activity; this dual-site design protects cells from oxidative stress and is generalizable to other metals such as Cu, Mn, Co, Zn, and Ni [34].

Visible light drives a large share of the solar spectrum, so Ag/AgX (X = Cl, Br, I) components are used to broaden absorption via surface plasmon resonance and to trap electrons, which suppresses recombination and adds intrinsic antimicrobial action [35]. Ag/ZnO@C hollow structures derived from Ag^+-incorporated zeolitic imidazolate framework show about tenfold faster Rhodamine B removal than ZnO. They efficiently inactivate *E. coli* under light thanks to plasmon-enhanced absorption and charge separation improved by well-defined ZnO/Ag interfaces (Fig. 4b) [36]. Quaternized chitosan supported Ag–TiO_2 (QCS@Ag–TiO_2) combines abundant adsorption sites, N-doped TiO_2 for charge separation, and Ag nanoparticles for charge transfer, plasmonic, and photothermal effects (Fig. 4c). It provides 96.4% degradation of low-temperature Sodium Dodecyl Benzene Sulfonate (SDBS) wastewater in 180 min and completely *E. coli* in 120 min [37]. Co-doped Ag–Cu/TiO_2 prepared by sol–gel outperforms single-metal TiO_2 and the SODIS process for inactivation of *E. coli* and *Salmonella typhimurium* (Fig. 4d); copper loading and total catalyst dose dominate performance, and antibacterial activity persists even without light [38].

An Ag/AgCl–Bi_2MoO_6 system uses photo-formed plasmonic Ag to mediate electron transfer from Bi_2MoO_6 to AgCl while AgCl supplies interfacial sites for radical generation (Fig. 4a), giving superior visible-light disinfection supported by photoluminescence, photoelectrochemistry, and theory [39]. A nanocomposite of Ag, Zeolite Imidazole Framework-67 and graphene oxide (GO), Ag/ZIF-67@GO, activates peroxymonosulfate (PMS) under visible light that allows rapid phenol degradation and full inactivation of 10^6 CFU mL^{-1} *E. coli* in 15 min. The key reactive species are sulfate radicals ($SO_4^{\bullet-}$) and $^{\bullet}OH$, while superoxide contributes through photoinduced electron–hole generation. The catalyst is reusable with negligible Ag leaching [40].

In general, carbon-based composites with peroxidase-like activity show that metal coupling to conductive carbon frameworks accelerates electron transfer. Plasmonic resonance or heterojunction design allows for extending activity into the visible light range, and suppresses recombination, in order to efficiently convert H_2O_2 or PMS to $^{\bullet}OH$ and $SO_4^{\bullet-}$. Such materials are stable and reusable. However, their performance under realistic matrices that contain carbonate, chloride, and natural organic matter remains an open question. One more challenge for the future development is the management of potential Ag release, and integrating antimicrobial testing with ROS diagnostics to link the mechanism to disinfection outcomes.

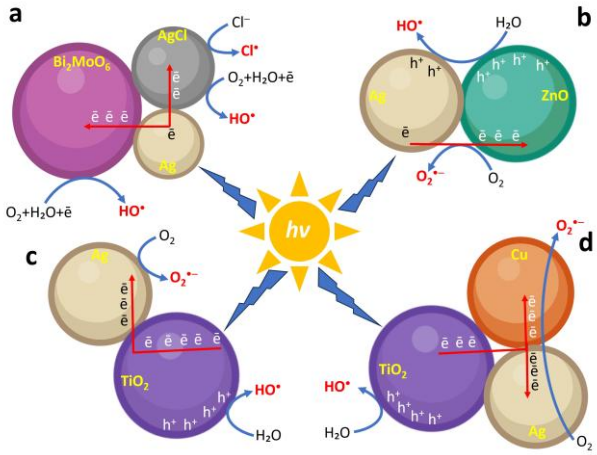

Fig. 4. Plasmon-assisted Ag composites under visible light: charge transfer and radical generation. a) Ag/AgCl–Bi_2MoO_6. Under hν, Photoactivated Ag mediates electron transfer to Bi_2MoO_6 and AgCl. Interfacial sites on Bi_2MoO_6 and AgCl generate radicals, giving $HO^{\bullet}$ and $Cl^{\bullet}$ and enhanced disinfection; b) Ag/ZnO. Visible light excites ZnO. Ag transfer e^- to ZnO. Electrons reduce O_2 to $O_2^{\bullet-}$, while holes oxidize H_2O to $HO^{\bullet}$; c) Ag/TiO_2. Ag acts as an electron sink and plasmonic absorber that improves light harvesting. Holes on TiO_2 oxidize H_2O to $HO^{\bullet}$, and electrons on Ag reduce O_2 to $O_2^{\bullet-}$; d) Ag–Cu/TiO_2. Ag and Cu cooperate in charge transfer. Cu^{2+}/Cu^{+} cycles promote redox reactions and Ag collects e^-. Both $O_2^{\bullet-}$ and $HO^{\bullet}$ form, and antibacterial activity can persist without light.

IV. Disinfection of wastewater using H_2O_2 and UV/visible radiation

Combining hydrogen peroxide with UV or visible light is an advanced oxidation process that generates short-lived reactive oxygen species, chiefly $HO^{\bullet}$, which rapidly damage membranes, proteins, and nucleic acids. Compared with chlorination, UV/H_2O_2 offers broad-spectrum antimicrobial action with a lower propensity for harmful disinfection by-products, making it a sustainable polishing step for wastewater reuse [41].

A 280 nm UV-LED plus H_2O_2 outperformed UV alone against a clinically relevant, multidrug-resistant *E. coli* ST131-A strain, which showed marked UV tolerance and photoreactivation. The addition of H_2O_2 boosted $HO^{\bullet}$ formation and provided residual oxidant to suppress regrowth [42]. When UVC-LEDs were compared with low-pressure mercury lamps (LPUV) for UV/H_2O_2 treatment of wastewater containing disinfection byproducts precursors and pharmaceutical and personal care products, UV dose governed removal, while H_2O_2 dose, dissolved organic carbon concentration, and

turbidity had smaller effects. After normalizing to UV dose, UVC-LED and LPUV achieved comparable performance despite the lower photoelectric efficiency of LEDs [43].

Modeling of reclaimed-water datasets indicated that far UV (222 nm) is more effective than 254 nm UV for disinfectant-resistant bacteria, particularly *Pseudomonas aeruginosa*. Combinations UV222/H_2O_2 or UV222/ peroxymonosulfate further enhanced antibacterial effect via radical mechanisms, but 100–200 mJ cm^{-2} of additional 222 nm dose was required to suppress regrowth. Biosafe operating windows of 300–500 mJ cm^{-2} light intensity were proposed, which are way above the 10–200 mJ cm^{-2} commonly used at reclaimed water treatment plants [44]. Polyethylene microplastics at 0.25–1.0 g L^{-1} reduced disinfection by both UV/H_2O_2 and ozonation; nevertheless, UV/H_2O_2 consistently achieved higher *E. coli* log-reductions than ozonation under comparable conditions, while effects on contaminants of emerging concern (CEC) removal were moderate for UV/H_2O_2 and smaller for ozonation (tested at high ozone doses) [45]. In secondary effluent treated by H_2O_2 and UV/Vis under optimized conditions, enterobacteria and heterotrophs were completely inactivated, and antibiotic resistance genes (ARG) markers (16S rRNA, bla_{tem}, *qnrS*, *intl1) were reduced. However, regrowth appeared after three days. Blending the treated effluent 1:1 with river water suppressed regrowth and met reuse standards for urban and agricultural applications.[46]

UV disinfection alone is also widely practiced. Collimated-beam experiments with a pure *Escherichia coli* culture showed that illumination with a power density of 0–20 mJ cm^{-2}, which is commonly applied in wastewater disinfection, induces approximately a 5.5-log reduction in the number of culturable cells [47]. Quantitative polymerase chain reaction (qPCR) is a rapid proxy for monitoring UV disinfection performance and clarifying how extensive genomic damage underpins loss of culturability.

According to a recent review [48], UV-LEDs and 222 nm excimer lamps are displacing low-pressure mercury lamps (LPUV) due to compactness, durability, and wavelength selectivity, with ongoing efforts to improve wall-plug efficiency and reactor design. For *Legionella pneumophila*, 255 nm LEDs achieved higher log-reductions at lower fluence than 265 or 280 nm, with strain-dependent susceptibility observed both in batch and point-of-entry flow devices [49]. Bench-scale studies indicate that, at projected 20% LED wall-plug efficiency, UV-LED reactors could consume 24.6–43.4% less power than LPUV systems for 30–40 mJ cm^{-2} doses, while delivering superior disinfection at small scale [50].

UV/H_2O_2 water treatment yields water with residual H_2O_2, which should be quenched to avoid increased chlorine demand during downstream purification steps. It can be done using granular activated carbon (GAC) that effectively decomposes H_2O_2. Basic surface functionalities correlate with faster quenching, and bicarbonate increases interfacial $HO^{\bullet}$ and persistent free radicals on GAC, accelerating decomposition in both model and real waters [51]. Residual H_2O_2 can hinder the removal of certain aldehydes and organic acids; behavior depends on GAC type, where removal pathways span adsorption, biodegradation, and catalytic decomposition, and H_2O_2 is largely quenched in the upper column layers during filtration [52].

Research in the field of practical application of wastewater disinfection using H_2O_2 and UV/visible radiation is quite active in recent years, and the main focus of recent works lies mostly in the search for optimal wavelengths and studies of effects on particular types of bacteria

V. Visible/solar photocatalysis with H_2O_2 as a co-oxidant (heterojunctions, plasmonics)

Visible and solar photocatalysis harvest a large fraction of sunlight and, when coupled with H_2O_2, proceed through routes analogous to photo Fenton that boost $HO^{\bullet}$ and related reactive oxygen species generation [53]. Heterojunction architectures, including type II, Z scheme, and especially S scheme, promote vectorial charge separation while preserving strong redox potentials, which accelerate H_2O_2 activation and pollutant oxidation. Plasmonic nanoparticles (Ag, Au, Cu) extend visible absorption through surface plasmon resonance (SPR), act as electron sinks/hot-carrier injectors, and suppress e^-/h^+ recombination. Structural motifs, like mesoporous and hierarchical frameworks, further improve mass transport and active-site exposure, enabling efficient degradation of dyes, pharmaceuticals, and pathogens under solar or visible irradiation [54].

S-scheme heterojunctions couple an oxidizing photocatalyst (OP) with a reducing photocatalyst (RP). Interfacial contact equalizes Fermi levels, bends bands, and drives selective recombination of OP-CB electrons with RP-VB holes. The retained OP-VB h^+ and RP-CB e^- maintain strong oxidative/reductive power, enabling both pathogen inactivation and two-electron O_2 reduction to H_2O_2 [55–57]. An inorganic/organic S-scheme made by anchoring CdS nanocrystals onto a pyrene-based conjugated polymer (PT) delivered an H_2 evolution rate of 9.28 mmol h^{-1} g^{-1} with an apparent quantum efficiency of 24.3%, verified by in-situ XPS and photo-Kelvin probe [59]. While focused on H_2, it exemplifies S-scheme carrier management relevant to ROS chemistry. A ZnO/WO_3 S-scheme achieved H_2O_2 production at 6788 μmol L^{-1} h^{-1}, proceeding mainly via direct two-electron O_2 reduction. The interfacial internal electric field was identified as the key to efficient charge separation and reductive power retention [60]. Flower-like $CdS/K_2Ta_2O_6$ constructed via vacancy anchoring reached 160.89 μmol g^{-1} h^{-1} H_2O_2 in water/air (no sacrificial agents) and 346.31 μmol g^{-1} h^{-1} under $O_2^{\bullet-}$-saturated conditions. The S-scheme pathway was confirmed by in-situ XPS, EPR, and DFT [61]. For direct disinfection, a CuS/Bi_5O_7I S-scheme achieved complete *E. coli* inactivation (5×10^8 CFU mL^{-1}) within 180 min under visible light. Primary acting species were $O_2^{\bullet-}$ and h^+ (hole). Clear evidence of membrane disruption and leakage of K^+, proteins, and DNA were also obtained [62].

Plasmon-enhanced Ag/g-C_3N_4 efficiently generates H_2O_2 under solar and visible light. With ultrasonic piezo-

activation and air bubbling, a 5% Ag loading achieved 3964.89 μmol g^{-1} h^{-1} (solar piezo-photocatalysis) and 2552.37 μmol g^{-1} h^{-1} (visible light), attributed to SPR-assisted light harvesting, electron trapping, and piezo-field-aided charge separation.

Mechanistic tests showed $O_2^{\bullet-}$ dominates H_2O_2 formation, while HO$^\bullet$ arises secondarily from H_2O_2 decomposition. The catalyst retained ~98.6% activity over five cycles [63]. Beyond disinfection per se, graphene-modified TiO_2 with ultrathin N-doped graphene (TiO_2/NG) illustrates how conductive 2D cocatalysts and pyridinic-N sites enhance charge separation, adsorption/activation (e.g., CO_2 in that study), and photothermal contributions—principles transferable to water-phase ROS generation and H_2O_2 co-oxidant chemistry [58].

SPR in Ag/Au/Cu nanoparticles concentrates electromagnetic fields and produces energetic carriers that couple to semiconductor bands, extending action into the visible, deepening H_2O_2 activation, and strengthening ROS fluxes [64]. Combining plasmonic layers with S-scheme or Z-scheme junctions maximizes both absorption and charge-use efficiency, while mesoporous/hierarchical morphologies sustain mass transfer and limit fouling.

For water disinfection and pollutant control, best practice is to report photon-normalized metrics (e.g., apparent quantum yields for H_2O_2), monitor H_2O_2 residuals and regrowth, and quantify ROS (HO$^\bullet$/$O_2^{\bullet-}$/$^1O_2$) to connect materials design with mechanisms and outcomes. Visible/solar photocatalysis with H_2O_2 co-oxidant can become a robust and scalable route to advanced oxidation and microbial control.

VI. Electro- and photoelectro-Fenton with in situ H_2O_2

Electro-Fenton (EF) and photoelectro-Fenton (PEF) processes generate HO$^\bullet$ in situ by combining cathodic H_2O_2 electrosynthesis with fast Fe^{2+}/Fe^{3+} cycling (Fig. 5). At the gas-diffusion or carbon cathode, dissolved O_2 is reduced via the two-electron pathway to H_2O_2; adsorbed HO$^\bullet$ can also form at "non-active" anodes and, on Boron-doped diamond (BDD), as physisorbed HO$^\bullet$. In PEF, UV/visible light photoreduces Fe^{3+} to Fe^{2+} (e.g., Fe–OH or Fe–EDDS), accelerating bulk HO$^\bullet$ generation [65].

A key limitation of EF is the drop in performance near neutral pH due to iron precipitation. Using a low dose of soluble Fe–EDDS (1:1) as the catalyst restored activity at pH 7.0 for triclopyr degradation in Na_2SO_4: under UVA-PEF and solar PEF, photoreduction regenerated Fe^{2+} and enhanced removal relative to EF. Hydroxyl radicals produced both at the anode and in the bulk dominated oxidation. BDD anodes mineralized more efficiently than IrO_2, although at a higher energy cost. Catalyst concentration, current density, and chloride strongly affected outcomes, and solar PEF further accelerated triclopyr and catalyst decay; a pathway via heteroaromatic intermediates, aliphatic fragments, and small acids was proposed [66].

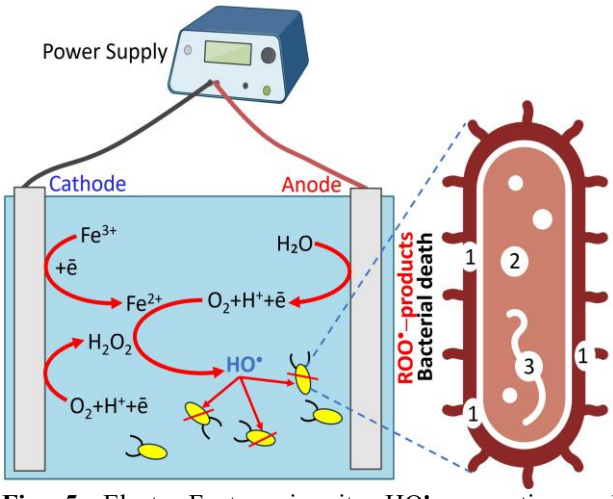

Fig. 5. Electro-Fenton: in situ HO$^\bullet$ generation and bacterial inactivation pathways. A DC-powered cell forms H_2O_2 and Fe^{2+} at the cathode; Fe^{2+} reacts with H_2O_2 in the bulk to generate HO$^\bullet$ and regenerate Fe^{3+}; the anode oxidizes water to O_2. The resulting HO$^\bullet$ reaches cells and inactivates them. 1 – membrane damage: lipid peroxidation, higher permeability, loss of potential, leakage; 2 – protein damage: oxidation of residues, disulfide disruption, carbonylation, aggregation; 3 – DNA damage: single and double strand breaks, base lesions, abasic sites, blocked replication.

A factorial design was used to optimize the treatment of greywater containing linear alkylbenzene sulfonate (LAS). Bench-scale AO–H_2O_2 (BDD anode; carbon–PTFE air-diffusion cathode) achieved 76% LAS removal and 52% TOC abatement under optimal settings. PEF with 5 mg L^{-1} Fe^{2+} at 77.5 mA cm^{-2} reached 63% LAS removal and 78% TOC abatement. The optimized recipe translated to solar PEF, yielding 70% LAS removal and 55% mineralization after 240 min, with acute-toxicity reduction confirmed by *Artemia salina*. Among the evaluated EAOPs, solar PEF offered the best trade-off between efficacy and scalability [67].

A binder-free, electrospun Fe^{2+} sustained-release electrode enabled a steady Fe^{2+} supply within an EF reactor treating aniline wastewater. The nanofibrous architecture dispersed and nanoconfined Fe^{2+}, promoted homogeneous/heterogeneous coexistence, and improved mass transfer in a flow-through configuration, achieving 96.1% aniline removal in 120 min with $k = 0.027\ min^{-1}$—about 6.5× faster than conventional setups. Computational fluid dynamics simulations clarified velocity fields and contact between pollutants and catalytic sites, informing scale-up and reactor optimization [68].

Progress in neutral-pH catalysis (Fe–EDDS), solar PEF, durable air-diffusion cathodes, and sustained-release iron sources is moving EF/PEF toward practical water reuse. Future priorities include energy benchmarking against UV/H_2O_2, iron-leaching control, matrix tolerance (chloride, carbonate, NOM), and management of residual oxidants, all within the mechanistic framework of Fig. 2.

VII. Side-effects, ecotoxicology, by-products, and safety

Advanced oxidation processes (AOPs) can generate short-lived ROS that inactivate microbes but also transform contaminants into aldehydes, low-molecular-weight acids, halogenated by-products in chloride-rich waters, and other intermediates that may be more toxic or persistent than the parent compounds. Nanoparticle release or metal leaching from heterogeneous catalysts adds a secondary-pollution pathway and can decrease catalyst durability. Robust assessment, therefore requires targeted chemistry (parent and transformation products), non-target mass-spectroscopy screening, and ecotoxicity tests across trophic levels, together with life-cycle and energy analyses.

UV-based AOPs alter bacterial cells and extracellular DNA. In comparative tests, removal of extracellular ARGs followed the order UV/chlorine > UV/H_2O_2 > UV/peracetic acid, driven by HO$^{\bullet}$ and, most strongly, by reactive chlorine species (RCS) [69]. For intracellular ARGs, UV/H_2O_2 provided little benefit over UV alone because cellular components scavenge radicals, whereas UV/peracetic acid showed modest synergy via intracellular HO$^{\bullet}$. UV/chlorine achieved the strongest overall effect, but the gain comes with an RCS/DBP trade-off. Flow cytometry linked membrane damage primarily to chlorine oxidation; qPCR provided sensitive DNA-damage readouts, illustrating the need to pair culture-based assays with molecular endpoints [69].

Beyond UV-AOPs, sulfate-radical systems can suppress both ARB and ARGs. A sulfidated nano-zerovalent iron/persulfate process achieved impressive ~7.8-log ARB inactivation within 10 min and ~8-log removal of extracellular ARGs within 5 min in both drinking-water and wastewater matrices; intracellular ARGs diminished more slowly (~4-log in 60 min), consistent with shielding by damaged cell debris [71]. Results highlight both the promise and the limits of $SO_4^{\bullet-}$ pathways for simultaneous ARB and ARG control in real waters.

Metal dissolution (Fe, Cu, Mn, Co, Ni) from heterogeneous catalysts can breach reuse standards, increase ecotoxicity, and erode long-term performance. Leaching depends on pH, oxidant dose, redox potential, and hydrodynamics. Mitigation includes stronger metal–support interactions, encapsulation or core–shell designs, operation in pH windows that minimize solubility, and routine leachate monitoring (ICP-MS) alongside organismal toxicity tests on treated effluents [72].

Safe deployment hinges on controlled handling of oxidants, UV shielding, and electrode integrity. Residual H_2O_2 after UV/H_2O_2 must be quenched (e.g., by granular activated carbon or catalytic media) to avoid downstream chlorine demand and distribution-system impacts (see Sec. 6). For UV/chlorine, DBP formation needs explicit tracking and, if used, should be paired with DBP mitigation. For electro-/photoelectro-Fenton, neutral-pH chelates (e.g., Fe–EDDS) reduce precipitation risk but require assessment of chelate persistence. Process upscaling should include energy benchmarking and materials durability (erosion, catalyst shedding).

Design AOP trains that couple selective oxidation with downstream polishing/adsorption to capture transformation products; report mass balances and toxicity reduction, not only parent removal. For antimicrobial endpoints, combine culture counts with qPCR (ARGs, long-amplicon DNA damage) and cytometry to detect sub-lethal injury and regrowth potential. Finally, prioritize catalysts with low leaching, document effluent ecotoxicity, adopt operating windows that minimize by-products while achieving the target disinfection level, and balance efficacy (for example, the contribution of reactive chlorine species in UV/chlorine) with safety and regulatory constraints [69–72].

VIII. Outlook: materials, devices, and sustainability

Next-generation AOP materials should couple high activity with selectivity, durability, and low leaching under realistic water chemistries. Promising directions include defect- and dopant-engineered semiconductors, spinel ferrites and PB/PBA frameworks with stabilized Fe redox cycling, and carbon-anchored single-atom sites that activate H_2O_2 efficiently at circumneutral pH. Green synthesis using bio-templates or waste-derived precursors, and architectures that ease recovery (magnetic cores, supported films), can lower environmental burden while improving service life.

Rational device design is as important as material discovery. Photoelectrochemical cells, electro-/photoelectro-Fenton reactors with in situ H_2O_2, and UV/H_2O_2 contactors should be optimized for mass transfer, photon use, and energy efficiency, with control of residual oxidants and regrowth. Portable and modular reactors powered by renewables (solar PV, wind) are poised to expand decentralized reuse while reducing operating costs.

A continuous UV/H_2O_2 tubular photoreactor used as pretreatment improved the biodegradability of polyvinyl alcohol wastewaters. Response-surface optimization identified an operating window (≈665 mg L^{-1} PVA, 390 mg L^{-1} H_2O_2, 59 mL min^{-1}) that raised the effluent BOD_5/COD ratio from 0.15 to 0.53, with model predictions validated to within ±5% [73]. This illustrates how UV/H_2O_2 can be positioned upstream of biology to shift from complete mineralization to cost-effective bioconversion.

Comparisons of UV-C LEDs with mercury low-pressure lamps show higher bench-scale inactivation kinetics for LEDs but a strong dependence on duty cycle and electricity pricing. Continuous WWTP operation currently favors Hg lamps on environmental and economic metrics, whereas intermittent or decentralized use cases favor LEDs in most impact categories [74]. At full scale, a 280 nm LED reactor delivered consistent 3-log reductions of *E. coli* and total coliforms across varied UV transmittance, with delivered fluence (~28 mJ cm^{-2} at 817 m^3 d^{-1}) matching pre-installation audits, confirming technical viability and the value of bench-to-plant fluence validation [75].

A comparative life cycle assessment (LCA) of

municipal disinfection during operation ranked low-pressure UV as the lowest impact, followed by chlorination; ozonation and UV-LEDs were the highest, primarily due to electricity demand. The electricity mix altered absolute impacts but did not change the ranking, emphasizing the need for energy-efficient reactors and cleaner grids [76]. Early-stage techno-economic analysis and LCA should therefore guide material choice, reactor configuration, and operating set-points.

Priorities include neutral-pH catalysis with minimal leaching, photon- and electron-efficient reactors that manage residual oxidants, robust control of regrowth, and validated performance in complex matrices containing carbonate, chloride, NOM, and microplastics. Standardized reporting should include photon-normalized metrics, iron and by-product speciation, toxicity reduction, and long-cycle stability. Integrating renewable power, modular hardware, and green synthesis will help balance high performance with environmental sustainability.

Conclusions

This review assembles a coherent picture of hydrogen peroxide assisted advanced oxidation processes for water and wastewater treatment and links mechanistic steps to engineering choices. Across homogeneous and heterogeneous Fenton and photo-Fenton systems, peroxidase-like nanozymes, carbon co-catalysts, and photolytic UV or solar routes, the dominant constraints arise from oxidant activation versus self-scavenging, metal redox cycling, mass transfer, and the influence of pH and matrix constituents. A harmonized benchmarking scheme that combines energy per order, oxidant utilization efficiency, photon-normalized kinetics, mineralization selectivity, and durability with leaching control enables fair comparison and reveals conditions where each platform performs best. Actionable design rules emerge from this synthesis. Materials should present accessible and stable active sites, tuned electronic structure and defects, and resistance to dissolution. Reactors should manage optical paths, mixing, and residence time, while enabling oxygen reduction to hydrogen peroxide where relevant. Operation should target mildly acidic and buffered windows, adaptive hydrogen peroxide dosing, and matrix-aware pretreatment in order to suppress by-products and improve selectivity. Safe and scalable deployment requires rigorous attention to by-product formation and to catalyst stability. Staged oxidant delivery, in situ hydrogen peroxide generation in electro-Fenton architectures, and closed-loop monitoring reduce risk in complex waters. Integration with renewable power and modular photoelectrochemical or photolytic devices can lower energy and maintenance burdens and can support decentralized treatment. Clear reporting standards are essential for progress. Photon accounting, transparent optical specifications, standardized stability and leaching protocols, and cost and life-cycle disclosures should accompany performance data. Open datasets and machine-readable benchmarks will accelerate discovery and allow reproducible comparisons across laboratories. Future work should couple mechanistic modeling with operando diagnostics, develop control strategies that learn from water matrix variability, and validate durability at pilot and full scale. With these practices, hydrogen peroxide based advanced oxidation processes can deliver efficient, safe, and sustainable treatment from bench to real-world implementation.

Funding

This work was supported by the Ministry of Education and Science of Ukraine (project number 0124U000479).

Consent to participate

The authors declare their consent for publication.

Declaration of competing interest

The authors promulgate that they have no known competing financial profits or personal relationships that could have appeared to affect the results reported in this manuscript.

Husak V.V. – Candidate of Biological Sciences, Associate Professor of the Department of Biochemistry and Biotechnology;
Shvadchak V.V. – PhD, Associate Professor of the Department of Biochemistry and Biotechnology;
Soltys L.M. – Candidate of Chemical Sciences, Associate Professor of the Department of Chemistry.

[1] P. Kokkinos, D. Venieri, D. Mantzavinos, *Advanced Oxidation Processes for Water and Wastewater Viral Disinfection. A Systematic Review*, Food and Environmental Virology, 13, 283 (2021); https://doi.org/10.1007/s12560-021-09481-1.

[2] D. Wang, L. Cai, S. Song, S. Giannakis, J. Ma, D. Vione, C. Pulgarin, *Bacterial inactivation in sunlit surface waters is dominated by reactive species that emanate from the synergy between light, iron, and natural organic matter*, Applied Catalysis B: Environmental., 343, 123573 (2024); https://doi.org/10.1016/j.apcatb.2023.123573.

[3] P.B. Vilela, R.P. Mendonça Neto, M.C.V.M. Starling, A. da S. Martins, G.F.F. Pires, F.A.R. Souza, C.C. *Amorim, Metagenomic analysis of MWWTP effluent treated via solar photo-Fenton at neutral pH: Effects upon microbial community, priority pathogens, and antibiotic resistance genes*, Science of the Total Environment., 801, 149599 (2021); https://doi.org/10.1016/j.scitotenv.2021.149599.

[4] Y. Ahmed, J. Zhong, Z. Yuan, J. Guo, *Roles of reactive oxygen species in antibiotic resistant bacteria inactivation and micropollutant degradation in Fenton and photo-Fenton processes*, Journal of Hazardous Materials, 430, 128408 (2022); https://doi.org/10.1016/j.jhazmat.2022.128408.

[5] Y. Wu, A. Bianco, M. Brigante, W. Dong, P. De Sainte-Claire, K. Hanna, G. Mailhot, *Sulfate Radical Photogeneration Using Fe-EDDS: Influence of Critical Parameters and Naturally Occurring Scavengers*, Environmental Science and Technology, 49, 14343–14349 (2015); https://doi.org/10.1021/acs.est.5b03316.
[6] N. Thomas, D.D. Dionysiou, S.C. Pillai, *Heterogeneous Fenton catalysts: A review of recent advances*, Journal of Hazardous Materials. 404, 124082 (2021); https://doi.org/10.1016/j.jhazmat.2020.124082.
[7] X. Huang, N. Zhu, F. Mao, Y. Ding, S. Zhang, H. Liu, F. Li, P. Wu, Z. Dang, Y. Ke, *Enhanced heterogeneous photo-Fenton catalytic degradation of tetracycline over yCeO2/Fh composites: Performance, degradation pathways, Fe2+ regeneration and mechanism*, Chemical Engineering Journal, 392 123636 (2020); https://doi.org/10.1016/j.cej.2019.123636.
[8] R. Zhu, Y. Zhu, H. Xian, L. Yan, H. Fu, G. Zhu, Y. Xi, J. Zhu, H. He, *CNTs/ferrihydrite as a highly efficient heterogeneous Fenton catalyst for the degradation of bisphenol A: The important role of CNTs in accelerating Fe(III)/Fe(II) cycling*, Applied Catalysis B: Environmental., 270, 118891 (2020); https://doi.org/10.1016/j.apcatb.2020.118891.
[9] Y. Cheng, S. Zhang, Z. Wang, B. Wang, J. You, R. Guo, H. Zhang, *Review on spinel ferrites-based materials (MFe2O4) as photo-Fenton catalysts for degradation of organic pollutants*, Separation and Purification Technology, 318, 123971 (2023); https://doi.org/10.1016/j.seppur.2023.123971.
[10] Y. Xiang, Y. Huang, B. Xiao, X. Wu, G. Zhang, *Magnetic yolk-shell structure of ZnFe2O4 nanoparticles for enhanced visible light photo-Fenton degradation towards antibiotics and mechanism study*, Applied Surface Science, 513, 145820 (2020); https://doi.org/10.1016/j.apsusc.2020.145820.
[11] M. Usman, A. Ahmed, Z. Ji, B. Yu, M. Rafiq, Y. Shen, H. Cong, *Enhanced heterogenous photo-Fenton degradation of tetracycline in aqueous medium by visible light responsive sulphur dopped zinc ferrite nanoparticles*, Materials Today Chemistry, 26 (2022); https://doi.org/10.1016/j.mtchem.2022.101003.
[12] A. Kalam, A.G. Al-Sehemi, M. Assiri, G. Du, T. Ahmad, I. Ahmad, M. Pannipara, *Modified solvothermal synthesis of cobalt ferrite (CoFe2O4) magnetic nanoparticles photocatalysts for degradation of methylene blue with H2O2/visible light*, Results in Physics, 8, 1046 (2018); https://doi.org/10.1016/j.rinp.2018.01.045.
[13] M. Ismael, M. Wark, *Photocatalytic activity of CoFe2O4/g-C3N4 nanocomposite toward degradation of different organic pollutants and their inactivity toward hydrogen production: The role of the conduction band position*, FlatChem., 32, 100337 (2022); https://doi.org/10.1016/j.flatc.2022.100337.
[14] Y. Sun, J. Zhou, D. Liu, X. Li, H. Liang, *Enhanced catalytic performance of Cu-doped MnFe2O4 magnetic ferrites: Tetracycline hydrochloride attacked by superoxide radicals efficiently in a strong alkaline environment*, Chemosphere, 297 (2022); https://doi.org/10.1016/j.chemosphere.2022.134154.
[15] S. Kanithan, N. Arun Vignesh, K.M. Katubi, P.S. Subudhi, E. Yanmaz, J. Arockia Dhanraj, N.S. Alsaiari, M. Abualnaja, M. Sukumar, M. Sundararajan, S. Baskar, S. Sahu, C.S. Dash, *Enhanced optical, magnetic, and photocatalytic activity of Mg2+ substituted NiFe2O4 spinel nanoparticles*, Journal of Molecular Structure, 1265, 133289 (2022); https://doi.org/10.1016/j.molstruc.2022.133289.
[16] L. Liang, L. Ji, Z. Ma, Y. Ren, S. Zhou, X. Long, C. Cao, *Application of Photo-Fenton-Membrane Technology in Wastewater Treatment: A Review*, Membranes, 13 1 (2023); https://doi.org/10.3390/membranes13040369.
[17] S. Lee, B. Bayarkhuu, Y. Han, H.W. Kim, S. Jeong, C. Boo, J. Byun, *Multifunctional photo-Fenton-active membrane for solar-driven water purification*, Journal of Membrane Science, 660, 120832 (2022); https://doi.org/10.1016/j.memsci.2022.120832.
[18] C. Yan, Z. Cheng, J. Wei, Q. Xu, X. Zhang, Z. Wei, *Efficient degradation of antibiotics by photo-Fenton reactive ceramic membrane with high flux by a facile spraying method under visible LED light*, Journal of Cleaner Production, 366, 132849 (2022); https://doi.org/10.1016/j.jclepro.2022.132849.
[19] J. Gao, S. Ma, M. Xu, M. Yuan, J. Li, J. Xue, M. Wang, *Photo-Fenton superwettable NiFe2O4/TA/PVDF composite membrane for organic pollutant degradation with successively oil-in-water separation*, Chemosphere, 286, 131705 (2022); https://doi.org/10.1016/j.chemosphere.2021.131705.
[20] X. Dong, X. Liu, M. Cheng, D. Huang, G. Zhang, W. Wang, L. Du, G. Wang, H. Liu, *Prussian blue and its analogues: Reborn as emerging catalysts for a Fenton-like process in water purification*, Coordination Chemistry Reviews, 482 (2023); https://doi.org/10.1016/j.ccr.2023.215067.
[21] X. Liu, W. Wang, H. Lin, Y. Shen, Q. Fang, F. Liu, *Construction of hierarchical Prussian blue microcrystal with high sunlight absorption for efficient photo-thermal degradation of organic pollutants*, Separation and Purification Technology, 269, 118724 (2021); https://doi.org/10.1016/j.seppur.2021.118724.
[22] Q. Wang, Y. Yang, S. Ma, J. Wu, T. Yao, *Preparation of Fe3O4@Prussian blue core/shell composites for enhanced photo-Fenton degradation of rhodamine B, Colloids and Surfaces A*, Physicochemical and Engineering Aspects, 606, 125416 (2020); https://doi.org/10.1016/j.colsurfa.2020.125416.
[23] S. Singh, P.C. Pandey, *Synthesis and application of functional Prussian blue nanoparticles for toxic dye degradation*, Journal of Environmental Chemical Engineering, 8, 103753 (2020); https://doi.org/10.1016/j.jece.2020.103753.
[24] J. Wei, M. Yuan, S. Wang, X. Wang, N. An, G. Lv, L. Wu, *Recent advances in metal organic frameworks for the catalytic degradation of organic pollutants*, Collagen and Leather, 5 (2023); https://doi.org/10.1186/s42825-023-00140-8.

[25] W. Xu, W. Xue, H. Huang, J. Wang, C. Zhong, D. Mei, *Morphology controlled synthesis of α-Fe2O3-x with benzimidazole-modified Fe-MOFs for enhanced photo-Fenton-like catalysis*, Applied Catalysis B: Environmental, 291, 120129 (2021); https://doi.org/10.1016/j.apcatb.2021.120129.

[26] S. Huang, Y. Wang, S. Qiu, J. Wan, Y. Ma, Z. Yan, Q. Xie, *In-situ fabrication from MOFs derived MnxCo3-x@C modified graphite felt cathode for efficient electro-Fenton degradation of ciprofloxacin*, Applied Surface Science, 586, 152804 (2022); https://doi.org/10.1016/j.apsusc.2022.152804.

[27] Y. Li, X. Li, B. Wang, *Constructing tunable coordinatively unsaturated sites in Fe-based metal-organic framework for effective degradation of pharmaceuticals in water: Performance and mechanism*, Chemosphere, 310, 136816 (2023); https://doi.org/10.1016/j.chemosphere.2022.136816.

[28] J. Jin, L. Li, L. Zhang, Z. Luan, S. Xin, K. Song, *Progress in the Application of Carbon Dots-Based Nanozymes*, Frontiers in Chemistry, 9, 1 (2021); https://doi.org/10.3389/fchem.2021.748044.

[29] J. Kong, F. Zhou, *Preparation and Application of Carbon Dots Nanozymes*, Antioxidants, 13 (2024); https://doi.org/10.3390/antiox13050535.

[30] D. Zhao, R. Wang, C. Zhang, X. Xiao, *Preparation of Carbon Dots with Peroxidase-like Activity and Their Application in Staphylococcus aureus Detection and Antimicrobial Susceptibility Test*, Langmuir, 41, 6408 (2025); https://doi.org/10.1021/acs.langmuir.5c00632.

[31] S. Zhuo, J. Fang, M. Li, J. Wang, C. Zhu, J. Du, *Manganese(II)-doped carbon dots as effective oxidase mimics for sensitive colorimetric determination of ascorbic acid*, Microchimica Acta, 186 (2019); https://doi.org/10.1007/s00604-019-3887-6.

[32] W. Kang, A. Lee, Y. Tae, B. Lee, J.S. Choi, *Enhancing catalytic efficiency of carbon dots by modulating their Mn doping and chemical structure with metal salts*, RSC Advances, 13, 8996 (2023); https://doi.org/10.1039/d3ra01001e.

[33] Y. Feng, J. Qin, Y. Zhou, Q. Yue, J. Wei, *Spherical mesoporous Fe-N-C single-atom nanozyme for photothermal and catalytic synergistic antibacterial therapy*, Journal of Colloid and Interface Science, 606, 826–836 (2022); https://doi.org/10.1016/j.jcis.2021.08.054.

[34] S. Chen, W. Lu, R. Xu, J. Tan, X. Liu, *Pyrolysis-free and universal synthesis of metal-NC single-atom nanozymes with dual catalytic sites for cytoprotection*, Carbon, 201, 439 (2023); https://doi.org/10.1016/j.carbon.2022.09.034.

[35] Y. Shi, J. Ma, Y. Chen, Y. Qian, B. Xu, W. Chu, D. An, *Recent progress of silver-containing photocatalysts for water disinfection under visible light irradiation: A review*, Science of the Total Environment, 804, 150024 (2022); https://doi.org/10.1016/j.scitotenv.2021.150024.

[36] B. Niu, D. Wu, J. Wang, L. Wang, W. Zhang, *Salt-sealing-pyrolysis derived Ag/ZnO@C hollow structures towards efficient photo-oxidation of organic dye and water-born bacteria*, Applied Surface Science, 528, 146965 (2020); https://doi.org/10.1016/j.apsusc.2020.146965.

[37] A. Wang, Q. Zhu, Z. Xing, *Multifunctional quaternized chitosan@surface plasmon resonance Ag/N-TiO2 core-shell microsphere for synergistic adsorption-photothermal catalysis degradation of low-temperature wastewater and bacteriostasis under visible light*, Chemical Engineering Journal, 393, 124781 (2020); https://doi.org/10.1016/j.cej.2020.124781.

[38] D. Pino-Sandoval, M. Villanueva-Rodríguez, M.E. Cantú-Cárdenas, A. Hernández-Ramírez, *Performance of Ag-Cu/TiO2 photocatalyst prepared by sol-gel method on the inactivation of Escherichia coli and Salmonella typhimurium*, Journal of Environmental Chemical Engineering, 8 (2020); https://doi.org/10.1016/j.jece.2020.104539.

[39] M. Li, D. Li, Z. Zhou, P. Wang, X. Mi, Y. Xia, H. Wang, S. Zhan, Y. Li, L. Li, *Plasmonic Ag as electron-transfer mediators in Bi2MoO6/Ag-AgCl for efficient photocatalytic inactivation of bacteria*, Chemical Engineering Journal, 382 (2020); https://doi.org/10.1016/j.cej.2019.122762.

[40] M. Kohantorabi, S. Giannakis, G. Moussavi, M. Bensimon, M.R. Gholami, C. Pulgarin, *An innovative, highly stable Ag/ZIF-67@GO nanocomposite with exceptional peroxymonosulfate (PMS) activation efficacy, for the destruction of chemical and microbiological contaminants under visible light*, Journal of Hazardous Materials, 413, 125308 (2021); https://doi.org/10.1016/j.jhazmat.2021.125308.

[41] L. Yang, H. Yang, S. Yin, X. Wang, M. Xu, G. Lu, Z. Liu, H. Sun, *Fe Single-Atom Catalyst for Efficient and Rapid Fenton-Like Degradation of Organics and Disinfection against Bacteria*, Small, 18, 1 (2022); https://doi.org/10.1002/smll.202104941.

[42] F. Hashemzadeh, A. Geppert, L.J. Jackson, J.J. Harrison, G. Achari, *Hydrogen Peroxide Augments the Disinfection Efficacy of 280 nm Ultraviolet LEDs against Antibiotic-Resistant Uropathogenic Escherichia coli Otherwise Tolerant to Germicidal Irradiation*, ACS Omega, (2025); https://doi.org/10.1021/acsomega.5c02971.

[43] D. Leong, H. Bin Chen, G.S. Wang, *Application of UVC-LED/H2O2 in wastewater treatments: treatment efficacy on disinfection byproduct precursors and micropollutants*, Sustainable Environment Research, 33 (2023); https://doi.org/10.1186/s42834-023-00194-7.

[44] R. Gao, S.H. Gao, J. Li, F. Huang, Y. Zhao, J. Xie, Y. Pan, W. Zhang, A. Wang, *Removal of disinfection residual bacteria in UV222, UV222/H2O2 and UV222/peroxymonosulfate systems: what is the safe usage for wastewater reclamation*, Water Research, 282, 123602 (2025); https://doi.org/10.1016/j.watres.2025.123602.

[45] M. Adeel, G. Maniakova, L. Rizzo, *Tertiary/quaternary treatment of urban wastewater by UV/H2O2 or ozonation: Microplastics may affect removal of E. coli and contaminants of emerging concern*, Science of the Total Environment. 907, 167940 (2024); https://doi.org/10.1016/j.scitotenv.2023.167940.
[46] A.L.R. Gomes, S. Ribeirinho-Soares, L.M. Madeira, O.C. Nunes, C.S.D. *Rodrigues, Disinfection of Secondary Urban Wastewater Using Hydrogen Peroxide Combined with UV/Visible Radiation: Effect of Operating Conditions and Assessment of Microorganism Competition*, Water (Switzerland), 17 (2025); https://doi.org/10.3390/w17040596.
[47] N. Rahman, S.R. Chaganti, R. Seth, D.D. Heath, *Comprehensive evaluation of UV inactivation of E. coli using multiple gene targets and real-time quantitative PCR*, Water Research X. 26, 100285 (2025); https://doi.org/10.1016/j.wroa.2024.100285.
[48] K.D. Rauch, S.A. MacIsaac, B. Reid, T.J. Mullin, A.J. Atkinson, A.L. Pimentel, A.K. Stoddart, K.G. Linden, G.A. Gagnon, *A critical review of ultra-violet light emitting diodes as a one water disinfection technology*, Water Research X, 25, 100271 (2024); https://doi.org/10.1016/j.wroa.2024.100271.
[49] H.Y. Buse, J.S. Hall, G.L. Hunter, J.A. Goodrich, *Differences in UV-C LED Inactivation of Legionella pneumophila Serogroups in Drinking Water*, Microorganisms, 10, 1 (2022); https://doi.org/10.3390/microorganisms10020352.
[50] S.A. MacIsaac, K.D. Rauch, T. Prest, R.M. Simons, G.A. Gagnon, A.K. Stoddart, *Improved disinfection performance for 280 nm LEDs over 254 nm low-pressure UV lamps in community wastewater*, Scientific Reports, 13, 1 (2023); https://doi.org/10.1038/s41598-023-34633-7.
[51] J. Zeng, M. Zhang, X. Qin, Y. He, X. Liu, Y. Zhu, Z. Liu, W. Li, H. Dong, Z. Qiang, J. Lian, *Quenching residual H2O2 from UV/H2O2 with granular activated carbon: A significant impact of bicarbonate*, Chemosphere, 354 (2024); https://doi.org/10.1016/j.chemosphere.2024.141670.
[52] Y. Tang, C.S. Lee, H. Walker, C. Gobler, O. Apul, A.K. Venkatesan, X. Mao, *Effect of residual H2O2 on the removal of advanced oxidation byproducts by two types of granular activated carbon*, Journal of Environmental Chemical Engineering, 9, 106838 (2021); https://doi.org/10.1016/j.jece.2021.106838.
[53] A. Nazir, P. Huo, H. Wang, Z. Weiqiang, Y. Wan, *A review on plasmonic-based heterojunction photocatalysts for degradation of organic pollutants in wastewater*, Journal of Materials Science, 58, 6474 (2023); https://doi.org/10.1007/s10853-023-08391-w.
[54] A. Amirjani, N.B. Amlashi, Z.S. Ahmadiani, *Plasmon-Enhanced Photocatalysis Based on Plasmonic Nanoparticles for Energy and Environmental Solutions: A Review*, ACS Applied Nano Materials, 6, 9085 (2023); https://doi.org/10.1021/acsanm.3c01671.
[55] H. Li, W. Wang, K. Xu, B. Cheng, J. Xu, S. Cao, *Solar-driven H2O2 production by S-scheme heterojunction photocatalyst*, Chinese Journal of Catalysis, 72, 24 (2025); https://doi.org/10.1016/S1872-2067(24)60257-3.
[56] W. Fang, L. Wang, *S-Scheme Heterojunction Photocatalyst for Photocatalytic H2O2 Production: A Review*, Catalysts, 13 (2023); https://doi.org/10.3390/catal13101325.
[57] L. Zhang, J. Zhang, H. Yu, J. Yu, *Emerging S-Scheme Photocatalyst*, Advanced Materials, 34, 1 (2022); https://doi.org/10.1002/adma.202107668.
[58] L. Wang, B. Zhu, B. Cheng, J. Zhang, L. Zhang, J. Yu, *In-situ preparation of TiO2/N-doped graphene hollow sphere photocatalyst with enhanced photocatalytic CO2 reduction performance*, Chinese Journal of Catalysis, 42, 1648 (2021); https://doi.org/10.1016/S1872-2067(21)63805-6.
[59] C. Cheng, B. He, J. Fan, B. Cheng, S. Cao, J. Yu, *An Inorganic/Organic S-Scheme Heterojunction H2-Production Photocatalyst and its Charge Transfer Mechanism*, Advanced Materials, 33, 1 (2021); https://doi.org/10.1002/adma.202100317.
[60] Z. Jiang, B. Cheng, Y. Zhang, S. Wageh, A.A. Al-Ghamdi, J. Yu, L. Wang, *S-scheme ZnO/WO3 heterojunction photocatalyst for efficient H2O2 production*, Journal of Materials Science and Technology, 124, 193 (2022); https://doi.org/10.1016/j.jmst.2022.01.029.
[61] C. Lai, M. Xu, F. Xu, B. Li, D. Ma, Y. Li, L. Li, M. Zhang, D. Huang, L. Tang, S. Liu, H. Yan, X. Zhou, Y. Fu, H. Yi, *An S-scheme CdS/K2Ta2O6 heterojunction photocatalyst for production of H2O2 from water and air*, Chemical Engineering Journal, 452, 139070 (2023); https://doi.org/10.1016/j.cej.2022.139070.
[62] Z. Ma, W. Guo, K. Zhang, N. Wang, Z. Li, J. Li, *Construction of S-Scheme CuS/Bi5O7I Heterojunction for Boosted Photocatalytic Disinfection with Visible Light Exposure*, Molecules, 28 (2023); https://doi.org/10.3390/molecules28073084.
[63] H.P. Nguyen, H.N.M. Quang, H.C. Kung, L.T. Nguyen Huynh, T.L. Nguyen, S.J. You, B.W. Huang, M.T. Pham, G.P. Chang-Chien, *Plasmonic and piezo-photocatalytic enhancement in Ag/g-C3N4 for efficient visible-light-driven H2O2 production*, Optical Materials, 168, 117423 (2025); https://doi.org/10.1016/j.optmat.2025.117423.
[64] S. Ezendam, M. Herran, L. Nan, C. Gruber, Y. Kang, F. Gröbmeyer, R. Lin, J. Gargiulo, A. Sousa-Castillo, E. Cortés, *Hybrid Plasmonic Nanomaterials for Hydrogen Generation and Carbon Dioxide Reduction*, ACS Energy Letters, 7, 778 (2022); https://doi.org/10.1021/acsenergylett.1c02241.
[65] E. Brillas, J.M. Peralta-Hernandez, *The recent development of innovative photoelectro-Fenton processes for the effective and cost-effective remediation of organic pollutants in waters*, Chemosphere, 366, 143465 (2024); https://doi.org/10.1016/j.chemosphere.2024.143465.

[66] I.C. Da Costa Soares, R. Oriol, Z. Ye, C.A. Martínez-Huitle, P.L. Cabot, E. Brillas, I. Sirés, *Photoelectro-Fenton treatment of pesticide triclopyr at neutral pH using Fe(III)–EDDS under UVA light or sunlight*, Environmental Science and Pollution Research, 28, 23833 (2021); https://doi.org/10.1007/s11356-020-11421-8.

[67] P.R. dos Santos, M.E. de Oliveira Dourados, I. Sirés, E. Brillas, R.P. Cavalcante, P.S. Cavalheri, P.L. Paulo, D.R.V. Guelfi, S.C. de Oliveira, F. Gozzi, A. Machulek Junior, *Greywater treatment by anodic oxidation, photoelectro-Fenton and solar photoelectro-Fenton processes: Influence of relevant parameters and toxicity evolution*, Process Safety and Environmental Protection, 169, 879 (2023); https://doi.org/10.1016/j.psep.2022.11.058.

[68] J. Gao, Y. Zhou, W. Zhang, X. Yang, Y. Yao, C. Xiao, X. Guo, J. Qi, Z. Zhu, Y. Yang, J. Li, *Binder-Free Fe (II) Sustained-Release Electrode for Enhanced Flow-Through Electro-Fenton Degradation on Aniline-Containing Wastewater*, ACS ES&T Water, 4, 4625 (2024); https://doi.org/10.1021/acsestwater.4c00679.

[69] P. Petsi, K. Plakas, Z. Frontistis, I. Sirés, *A critical assessment of the effect of carbon-based cathode properties on the in situ electrogeneration of H2O2*, Electrochimica Acta, 470 (2023); https://doi.org/10.1016/j.electacta.2023.143337.

[70] F. Li, K. Liu, Y. Bao, Y. Li, Z. Zhao, P. Wang, S. Zhan, *Molecular level removal of antibiotic resistant bacteria and genes: A review of interfacial chemical in advanced oxidation processes*, Water Research, 254 121373 (2024); https://doi.org/10.1016/j.watres.2024.121373.

[71] Z. Yu, H. Rabiee, J. Guo, *Synergistic effect of sulfidated nano zerovalent iron and persulfate on inactivating antibiotic resistant bacteria and antibiotic resistance genes*, Water Research, 198, 117141 (2021); https://doi.org/10.1016/j.watres.2021.117141.

[72] W. Sun, S. Wang, Z. Yu, X. Cao, *Characteristics and application of iron-based materials in heterogeneous Fenton oxidation for wastewater treatment: a review*, Environmental Science: Water Research & Technology, 9, 1266 (2023); https://doi.org/10.1039/D2EW00810F.

[73] Z. Parsa, R. Dhib, M. Mehrvar, *Continuous UV/H2O2 Process: A Sustainable Wastewater Treatment Approach for Enhancing the Biodegradability of Aqueous PVA*, Sustainability (Switzerland), 16 (2024); https://doi.org/10.3390/su16167060.

[74] D. Pelayo, A. Hernández-Pellón, G. Santos, M. Rumayor, I. Ortiz, M.J. Rivero, *Performance of high-efficiency UV-C LEDs in water disinfection: Experimental, life cycle assessment, and economic analysis of different operational scenarios*, Journal of Environmental Management, 364 (2024); https://doi.org/10.1016/j.jenvman.2024.121442.

[75] S.A. MacIsaac, B. Reid, C. Ontiveros, K.G. Linden, A.K. Stoddart, G.A. Gagnon, *UV LED wastewater disinfection: The future is upon us*, Water Research X, 24, 100236 (2024); https://doi.org/10.1016/j.wroa.2024.100236.

[76] M.Z. Demir, H. Guven, M.E. Ersahin, H. Ozgun, M.E. Pasaoglu, I. Koyuncu, *Comparative Life Cycle Assessment of Four Municipal Water Disinfection Methods*, Sustainability (Switzerland), 16 (2024); https://doi.org/10.3390/su16146104.

В.В. Гусак, В.В. Швадчак, Л.М. Солтис

Каталітичні H_2O_2-системи для бактеріального знезараження стічних вод: Від ультрафіолетової/видимої синергії до електро-/фото-фентонних шляхів

Карпатський національний університет імені Василя Стефаника, Івано-Франківськ, Україна, viktor.husak@cnu.edu.ua

Процеси окиснення з використанням пероксиду водню є ключовими для водоочистки наступного покоління, проте прогрес гальмується фрагментованістю даних, відсутністю уніфікованих метрик і труднощами масштабування. У цьому огляді узагальнено механізми та ефективність гомогенних і гетерогенних каталізаторів Фентона та фото-Фентона, включно з аналогами пруської блакиті, MOF-похідними матеріалами, шпінелями, пероксидазоподібними наноензимами, вуглецевими ко-каталізаторами, а також фотолізними системами UV/H_2O_2 і видимого чи сонячного світла. Для уніфікації результатів застосовано схему бенчмаркінгу, що включає ефективність використання окисника, фотон-нормовану кінетику, вибірковість мінералізації та довговічність каталізаторів. Кінетичний аналіз показує обмеження, пов'язані з активацією H_2O_2 і його самопоглинанням, редокс-циклуванням металів, масопереносом та впливом pH і компонентів матриці (бікарбонат, галогеніди, природна органіка). Розглянуто контроль побічних продуктів і безпеку через поетапне дозування H_2O_2, попередню обробку стоків і in situ генерацію пероксиду у системах електро-Фентона. Техніко-економічний та життєво-цикловий аналіз виявляє, коли UV/H_2O_2 є оптимальним, коли сонячний фото-Фентон зменшує енергетичні витрати, а фотоелектрохімічні архітектури підвищують стабільність. Сформульовано правила для проєктування матеріалів, реакторів та умов роботи й запропоновано стандарти звітності для забезпечення прозорих порівнянь і прискореного впровадження.

Ключові слова: пероксид водню, удосконалені процеси окиснення, фото-фентонівський каталіз, УФ/H_2O_2, очищення стічних вод.